Norwegian Meteorological Institute
met.no

met.no report

no. 11/2004
Oceanography

Nondeterministic variability in the Skagerrak and the North Sea: A Pilot Study [1]

Arne Melsom

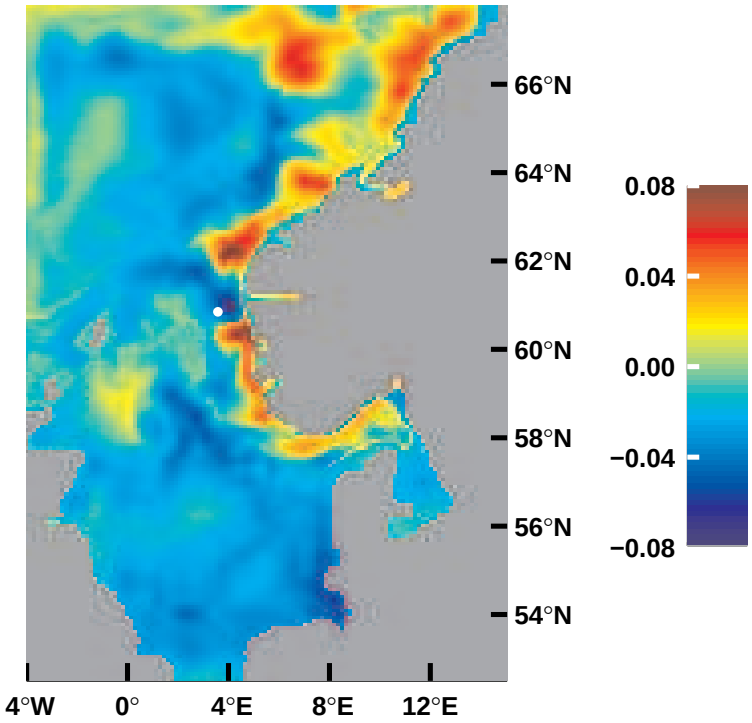

[1] This is an update of the printed version, a few minor errors have been corrected. Oslo, 30.09.2004.

Norwegian Meteorological Institute
met.no

report

Title	Date
Nondeterministic variability in the Skagerrak and the North Sea: A Pilot Study	1. 9. 2004
Section	**Report no.**
Oceanography	11
Author(s)	**Classification**
Arne Melsom	● Free ○ Restricted
	ISSN 1503-8025
Client(s)	**Client's reference**
Norwegian Research Council	146476/120

Abstract

The present study is an investigation of how small differences in initial conditions lead to differences in the results from an ocean circulation model. For this purpose, an eight-member ensemble was integrated for the period 1992 – 2001. No assimilation of synoptic observations was made. The integration domain includes the North Sea and the Skagerrak. The results from the analysis of the ensemble is presented in this report. By examining how the variability among the ensemble members converge as a function of ensemble size, we found that an ensemble should consist of at least six members in order to represent the bulk of the variability that can be expected due to small initial differences. The largest temporal variability in the results from one member, was found in the coastal wave guide off southern Norway. However, the fraction of ensemble variability due to flow instabilities relative to the total variability, was found to be highest in the frontal regions of the Norwegian Coastal Current and the Norwegian Atlantic current. There, small initial differences gives rise to differences in the model results that account for about 5% - 15% of the total variance. However, this result may well be scale-dependent, and that topic will be the subject of an upcoming publication.

Keywords

ensemble simulations, deterministic/nondeterministic variability, North Sea, Skagerrak

Disciplinary signature	Responsible signature
Øyvind Sætra	Thor Erik Nordeng

Cover: Baroclinic sea surface height anomaly on 18 November 2000. The white marker at 3° 35'E, 60° 51'N shows the position of the oil rig *West Venture* in the afternoon of this day. See also the discussion in the final section in this report.

Postal address P.O Box 43 Blindern N-0313 OSLO Norway

Office Niels Henrik Abels vei 40

Telephone +47 2296 3000

Telefax +47 2296 3050

e-mail: met.inst@met.no **internet:** met.no

Bank account 7694 05 00601

Swift code DNBANOKK

1 Introduction

Ocean circulation models have been run operationally at the Norwegian Meteorological Institute (*met.no*) for more than a decade (*Engedahl*, 1995; *Martinsen et al.*, 1997). The forecasts are produced by a suite of nested models that give results for separate or partially overlapping domains, on horizontal resolution that range from 20 km to 300 m. Originally, the main purpose of these simulations were to forecast extreme coastal sea levels due to storm surges. Subsequently, results for ocean currents have been given attention, first in order to forecast oil spill trajectories and the horizontal and vertical distribution of oil mass (*Martinsen et al.*, 1994; *Wettre et al.*, 2001) and later to simulate the drift of floating objects (*Sætra and Wettre*, 1999). In collaboration with the Institute of Marine Research, a biogeochemical module has also been added to the operational model, for the purpose of forecasting toxic algae bloom.

The ongoing activities at *met.no* in relation to operational ocean modeling include two topics that are vital in order to enhance the quality of our products. These activities are the inclusion of model validation on a routinely basis, and the implementation of algorithms for data assimilation in the simulations of ocean circulation. Although the present study is not a part of these activities, it is certainly related to them. The main purposes of this study are to quantify the uncertainty that arises due to errors in the initial fields, and to identify the geographical regions where such errors will be anomalously high and low.

The ocean circulation in the region of interest, the North Sea and the Skagerrak, is dominated by

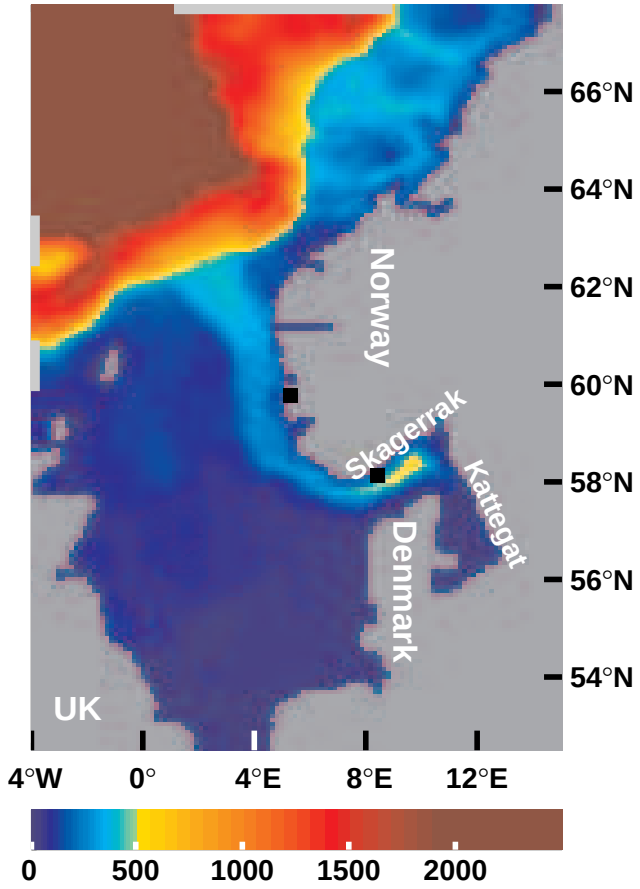

Figure 1: Model domain and the bottom topography in meters. The color coding is given by the color bar in the right panel. The land mask is given by the dark gray regions. Light gray lines along the western and northern boundaries indicate the position of the ports, see section 2 for details.

the inflow of salty Atlantic Water into the North Sea in the northeast, and the coastal currents that drain the freshwater fluxes from most European rivers north of the Alps. Further, from Figure 1 we observe that the ocean depths in the North Sea and the Skagerrak is about 100 m or less, with the exception of the Norwegian Trench, where the depth is about 500 m in its deepest parts. The circulation will be significantly affected by the wind forcing. This is not only due to small ocean depths, but it is also related to the high atmospheric variability at these latitudes, and the weak stratification that is found in much of the North Sea, particularly in the winter season.

The main coastal current in the region of interest is the wedge-shaped Norwegian Coastal Current that carries an average of 0.25-1 Sv (*Aure and Sætre*, 1981; *Dooley and Furnes*, 1981). From both observations and model studies, we know that mesoscale features like meanders and eddies are abundant on the front between the coastal current and the saltier Atlantic Water, see *e.g. Sætre* (1983) and *Røed and Fossum* (2004).

The variability of the ocean circulation on a time scale of days is dominated by the influence of atmospheric forcing. It has been suggested that extreme currents in the North Sea, with speeds exceeding 1 m/s, are related to outbreak of relatively fresh water masses from the Skagerrak. Such outbreak occurs when the wind relaxes or changes direction after a period with moderate or strong south to southwesterly winds that have piled up water in the Skagerrak, see e.g. *Furnes et al.* (2001).

Furnes et al. (2001) also discuss the relation between such events and the intensity of the mesoscale circulation in the aftermath of outbreak from the Skagerrak. If such a relation exists, then the intensity on the mesoscale is linked to the wind history. Further, it has been suggested that the position of ocean eddies in parts of this region could be linked to bottom topography features where vortex stretching occurs. Then, it is conceivable that it is possible to forecast ocean eddies without data assimilation. This possibility has motivated our present efforts, and will be investigated based on eddy resolving simulations, in an upcoming publication (*Melsom*, 2004). This study is undertaken by comparing results from an ensemble of simulations that differ only in the initial states. The present report presents the methodology that is used in this context, provides a theoretical background and discusses results from a set coarse resolution eddy permitting simulations.

This report is organized as follows: In section 2, the ocean circulation model is presented, then, some of the model results are discussed in section 3. The model initialization is pivotal in this context, and this is the topic of section 4. The methodology that is used in order to extract the pertinent information from the ensemble is presented in section 5. Then, the convergence of the ensemble variability as a function of the size of the ensemble is investigated in section 6, and the relationship between winds and oceanic variability is examined in section 7. Finally, some concluding remarks are provided in section 8.

2 The ocean model

The present study has been conducted using the HYbrid Coordinate Ocean Model (HYCOM). HYCOM has been developed based on the Miami Isopycnic Coordinate Ocean Model (MICOM) (*Bleck et al.*, 1992 and references therein). In HYCOM, the vertical coordinate is initially specified as target densities, and when the requested specification of layers can be met, the model layers are isopycnic. As a result, the isopycnic layers normally span the water column beneath the mixed layer in the deep, stratified ocean. There is a smooth transition to terrain-following coordinates in shallow coastal regions, and to z-level coordinates in the mixed layer and/or unstratified seas. The hybrid coordinate algorithm has been described in detail by *Bleck* (2002), and various specifications of the vertical coordinate have been described and tested by *Chassignet et al.* (2003).

Another novel feature in HYCOM is that the user may select one of several vertical mixing parameterizations. A detailed discussion of how HYCOM performs when five different mixed layer models are used, is given by *Halliwell* (2003). In MICOM, the only mixing scheme that was implemented was the Kraus-Turner slab mixed layer model (*Kraus and Turner*, 1967). Beneath the mixed layer, the dual entrainment parameterization by *McDougall and Dewar* (1998) was used in MICOM, and a modified version of this scheme that incorporates effects of vigorous turbulent mixing, has also been applied (*Hallberg*, 2000; *Shi et al.*, 2001).

For this study, the K-Profile Parameterization (KPP) closure scheme (*Large et al.*, 1994) was chosen. This is a semi-implicit scheme which includes a smooth transition from the diffusivity and viscosity profiles in the mixed layer to the diapycnal diffusivities and viscosities beneath the mixed layer. The KPP scheme includes parameterization of wind-induced mixing and surface buoyancy fluxes in the mixed layer, while beneath, the contribution from internal wave breaking, shear instability and double diffusion are taken into account.

Presently, the model was configured on a spherical grid, with a uniform horizontal resolution of 0.16° longitude by 0.08° latitude. This corresponds to about 9 km at the latitudes of the North Sea. The boundaries of the domain were set to 4°W in the west and 15.04°E in the east (corresponding to 121 grid nodes), and 52.5°N in the south and 67.78°N in the north (corresponding to 193 grid nodes), see Figure 1. Further, the simulations were conducted using seven hybrid layers. Their respective target densities were set to σ_t = 26.0, 26.4, 26.8, 27.2, 27.5, 27.8, 28.1 kg/m^{-3}. Wherever the hybrid coordinate adjustment algorithm produced *z* levels, the minimum and maximum thickness were set to 3 m and 12 m, respectively. The minimum depth was set to 30 m. Moreover, in order to reduce the constraint of the integration time step, the maximum depth was set to 2500 m. (The actual maximum depth in the present region is around 4000 m.)

The HYCOM simulations were performed with surface fluxes from the National Centers for Environmental Prediction (NCEP)/National Center for Atmospheric Research (NCAR) reanalysis data set. The model was spun up to a statistical equilibrium with a climatology of monthly mean surface fluxes. The climatology was calculated from reanalysis data for the period 1985–1991. Later, the simulations were continued using synoptic surface fluxes for the period 1992–2001. Surface fluxes of air temperature at 2 m, net total radiation, net long wave radiation, water vapor mixing ratio, wind speed, and momentum flux components toward east and north, were used to force the present simulations. The short wave radiation may penetrate beyond the upper model layer, depending on water clarity (*Jerlov*, 1976).

Along open boundaries, Newtonian relaxation was applied in sponge zones that extended six grids into the domain. In these zones, the relaxation time scale was set as a linear function of distance from the boundary, varying from 30 days at the boundary to 180 days at the innermost grids of the sponge zones. Also, the sea surface temperature and the sea surface salinity were nudged toward their climatological values. The monthly climatology for hydrography from the Institute for Marine Research and the Norwegian Meteorological Institute (*Engedahl et al.*, 1998) was applied for these purposes.

The simulations were performed with salinity as the prognostic sea state variable. In non-isopycnic layers, the density was also treated as a prognostic variable. The temperature was diagnosed from the equation of state.

In order to enhance the model's representation of the thermohaline variables, three additional actions were taken. First, in order to account for effects of the water mass exchange through the Baltic Straits, we defined a sponge zone that extended eleven grids in the southernmost region of the Kattegat in the model domain. At the three northernmost grids in this zone, the relaxation time scale was set to 40, 30, and 20 days, with the most gentle relaxation in the north. In the remaining part of

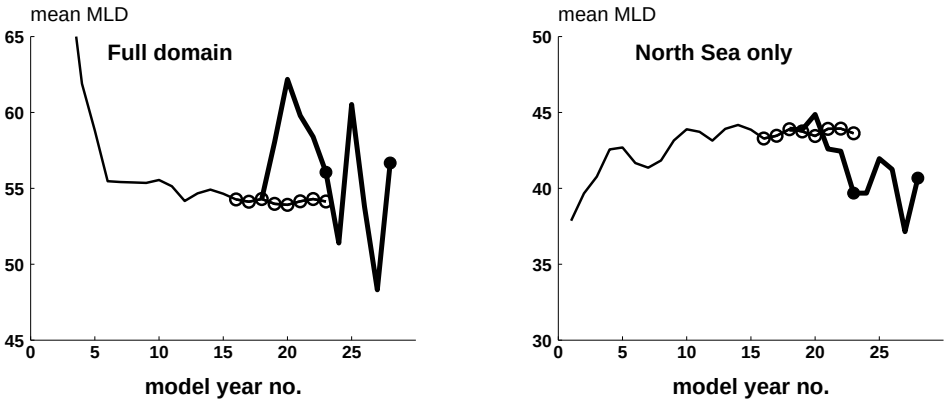

Figure 2: The spatial mean values (black lines, values in m along the vertical axes) of the mixed layer depth (MLD) in January, as a function of simulation year. Results obtained with climatological forcing are given by the thin lines, and the open circles correspond to the initial states for the eight ensembles members. The results from ensemble member *no*. 3, forced by synoptic atmospheric fields, are displayed by the thick lines. Results for January 1997 and 2002 are indicated by the full circles. Results for the full integration domain are shown in the left panel, while results for the North Sea are displayed in the right panel. The North Sea sub-domain extends to 61.5°N.

this zone, a relaxation time scale of 10 days was used. Second, in order to account for the flow of salty waters by the Norwegian Atlantic Current in the northern region, barotropic flow normal to the boundary was specified at three model ports, using the well-posed boundary conditions by *Browning and Kreiss* (1982). At two ports along the western boundary, the westward barotropic flow into the model domain was set to $0.4 \cdot 10^6$ m^3/s = 0.4 Sv (Sverdrup), equally partitioned (0.2 Sv at each port). Further, at a port along the northern boundary, the northward barotropic flow out of the domain was set to 0.4 Sv. The ports are indicated by light gray lines in Figure 1. Third, discharges from 41 rivers were parameterized as precipitation at the appropriate coastal grids, using climatological values.

As expected, the improved representation of the hydrography led to a more realistic flow field.

3 Model results

3.1 Initial state

The purpose of this study is to examine variability among an ensemble of ocean circulation simulations. As stated above, these members only differ in their initial states, which are taken from separate years of the climatologically forced simulation. In order for the ensemble members to properly represent the ocean circulation variability, it is essential that their initial states are taken from a period where the sea state is in a statistical equilibrium.

Here, we will present results for the mixed layer depth. In HYCOM the mixed layer depth is defined as the vertical level where the density contrast to the surface exceeds a threshold that corresponds to a temperature difference that is specified by the user. In the experiments that are considered in this report, this temperature difference was specified to be 0.2 °C.

The spatial mean value of the mixed layer thickness from January of each year, from the simulation with climatological forcing, is shown by the thin lines in Figure 2. Based on these results, we find that a statistical equilibrium is reached after 15 years (or earlier). Hence, the eight ensemble members were initiated from the January results after 16 – 23 years, indicated by the open circles in Figure 2.

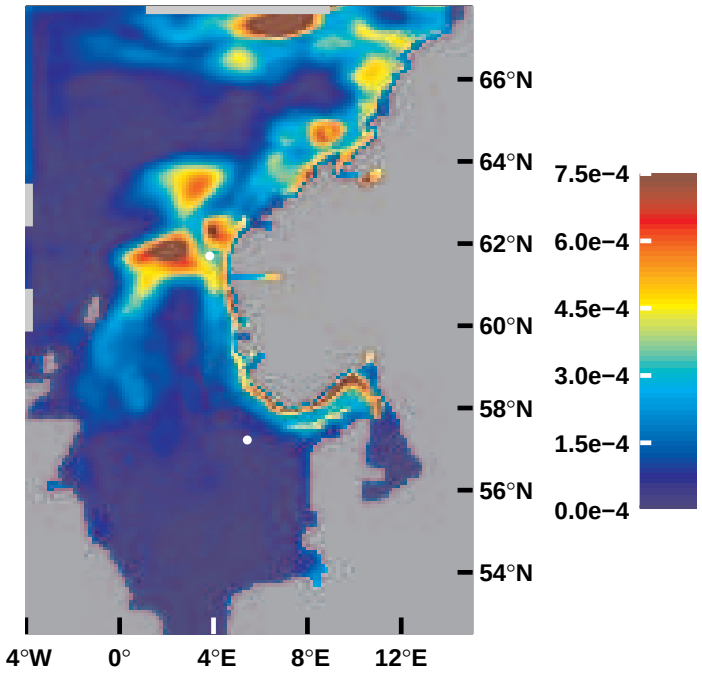

Figure 3: The variance of the baroclinic sea surface height ζ, based on offsets from the daily climatology. The color coding is shown by the color bar in the right panel, with values in m^2. This depiction is based on results from ensemble member *no.* 8. Two white markers indicate positions at which results will be examined in section 5.

The North Sea sub-domain, limited in the north by the 61.5°N latitude, was defined such that it almost entirely excludes the deep ocean of the southern Norwegian Sea. Thus, results for the North Sea will not be significantly affected by deep ocean variability.

The corresponding results from the ten year simulation with synoptic forcing from one of the ensemble members (*no.* 3) is shown by the thick lines in Figure 2. We note that the interannual variability is significantly larger for the full domain than it is for the North Sea sub-domain case. Moreover, from the results for the North Sea in the right panel of Figure 2, we find that there is a minor shift to a thinner mixed layer when the climatological atmospheric forcing is replaced by synoptic forcing.

Based on the results that are given above, and the results that are presented in section 3.1 below, we will restrict the analysis of the ensemble results to the period November 1996 – October 2001, *i.e.*, toward the final five years of the simulations.

3.2 Baroclinic sea surface height

HYCOM solves the depth integrated equations for volume transport and the corresponding sea surface height constituent separate from the equations for the remaining prognostic variables. Then, the local bottom pressure associated with the depth-dependent variables is constant in time, and we may define

$$\zeta = \frac{1}{g}\sum_{l=1}^{L}\frac{\Delta p_l}{\rho_l} - H_0 \tag{1}$$

where ρ_l is the density of layer l, and $\Delta p_l = p_{l+1} - p_l$ is the pressure difference from the bottom to the top of layer l (p_l is the pressure at the top of layer l). Furthermore, g is acceleration due to gravity, and H_0 is a reference depth. This quantity expresses the contribution from changes in the vertical density profile to the sea surface height. Hereafter, we shall refer to ζ as the baroclinic sea surface height.

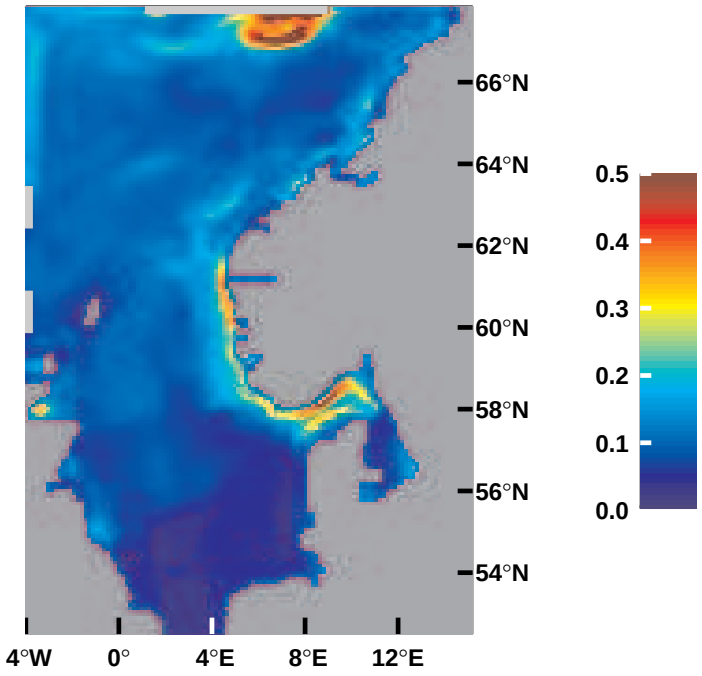

Figure 4: The mean eddy kinetic energy density. The color coding is shown by the color bar in the right panel, with values in m^3/s^2. This depiction is based on results from ensemble member *no.* 8.

Since the bottom pressure p_{L+1} in Equation (1) is time invariant, variations in the baroclinic sea surface height is equivalent to the local dynamic height anomaly. However, since the depth ranges over two orders of magnitude, as does the bottom pressure, spatial differences in the baroclinic sea surface height is not representative of corresponding differences in the dynamic height.

The local variance of the baroclinic sea surface height is depicted in Figure 3. These results were computed using offsets from the daily climatology. We note that the largest variances occur in the coastal wave guide, in the region north of the North Sea where the Norwegian Atlantic Current meets the Norwegian Coastal Current, and close to the outflow boundary in the far north.

3.3 Eddy kinetic energy

The eddy kinetic energy density for a wet grid node at time step n is

$$E_n^{eddy} = \frac{1}{2}\sum_{l=1}^{L}[h_{l,n}(\mathbf{v}_{l,n} - \bar{\mathbf{v}}_{l,d_n})^2] \tag{2}$$

where h_l is the thickness of layer l and $\mathbf{v}$ is the velocity vector for the baroclinic motion. The barotropic motion (the depth integrated motion) was disregarded, since the high frequency variability associated with the barotropic mode was not well-resolved with the present model output frequency of (2 days)$^{-1}$. (Synoptic forcing of ocean circulation in a shallow sea such as the North Sea, will lead to a barotropic mode which is of first order importance for the instant velocity field.)

Further, d_n in (2) is the decimal day of time step *n*, numbered from 1 January 1992 in cycles of 365.25 days, and

$$\bar{\mathbf{v}} = \frac{\widetilde{h\mathbf{v}}}{\tilde{h}} \tag{3}$$

is the layer-weighted velocity. Finally, $\tilde{h}$ and $\widetilde{h\mathbf{v}}$ are the daily climatologies for layer thickness and volume transport, respectively.

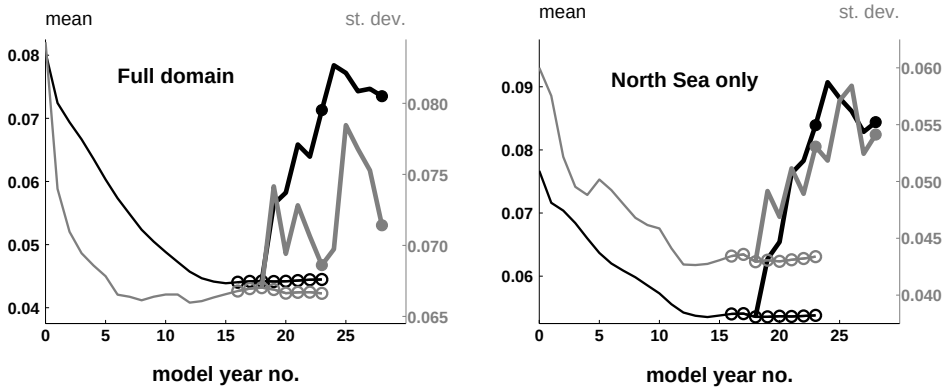

Figure 5: The spatial mean value (black lines) and the standard deviation (gray lines) of the baroclinic sea surface height in January, as a function of simulation year. Values along the vertical axes are in m. Results obtained with climatological forcing are given by the thin lines, and the open circles correspond to the initial states for the eight ensembles members. The results from ensemble member *no*. 3, forced by synoptic atmospheric fields, are displayed by the thick lines. Results for January 1997 and 2002 are indicated by the full circles. Results for the full integration domain are shown in the left panel, while results for the North Sea are displayed in the right panel.

4 Strategies for model initialization

The model initialization was discussed briefly in section 3.1, where the development of the mixed layer depth was examined. By definition, the variability of the mixed layer depth is only representative for the upper ocean variability. In order to examine the variability in the entire water column, results for the baroclinic sea surface height will be presented in this section.

The spatial means of the baroclinic sea surface height are depicted in Figure 5, analogously to the mixed layer results shown in Figure 2. Furthermore, results for the standard deviation are shown by gray lines, with values in m along the right axes.

It is obvious that the shift from climatological atmospheric forcing to synoptic forcing is not accompanied by a smooth transition in the ocean stratification. Due to this adjustment we will restrict the analysis to the period November 1996 – October 2001, as was indicated at the end of section 3.1.

This discrepancy led us to investigate alternative approaches for model initialization. This was done by considering two different aspects of the initialization. First, was the computation of the climatological fields conducted optimally? One issue that was investigated in this relation, was how values for the water vapor mixing ratio, r, were determined. In the original experiment, the climatology of r was set to the mean values of the synoptic fields for each month of the year. In HYCOM, r enters in the computation of the latent heat flux, in an expression that contains the product of r and the wind speed. Hence, a correct approach to calculating climatological values for r is to calculate the climatologies for this product and the wind speed climatology separately, and then set the climatology of r to the former divided by the latter. However, when this modification was introduced, the change in the model initialization was insignificant.

Another issue was how the wind speed climatology was determined. In HYCOM, the wind speed is used in order to calculate the friction velocity at the air-sea interface, u_*. Then various powers of u_* is used in the K-Profile Parameterization closure scheme. In the original experiment, the wind speed climatology was set to the mean values of the synoptic fields for each month of the year. As an alternative, the wind speed climatology was calculated from the square root of the mean squares of the synoptic wind speeds. The results for the baroclinic sea surface height when the model was

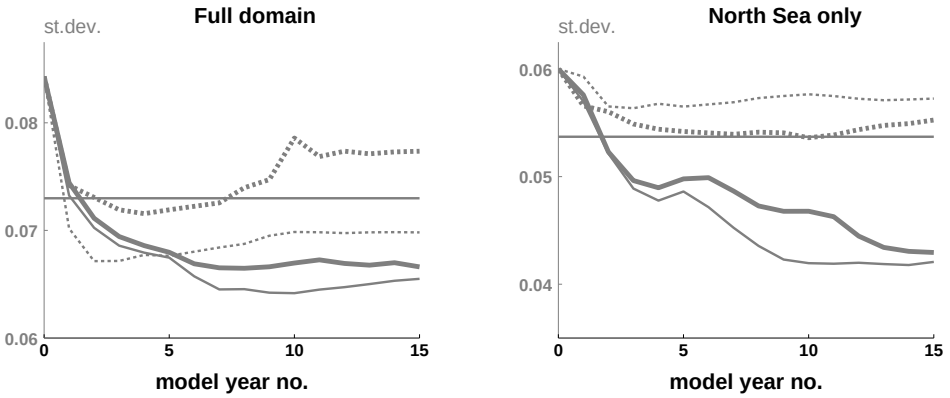

Figure 6: The standard deviation of the baroclinic sea surface height in January, as a function of simulation year. Values along the vertical axes are in m. Thick and thin full lines correspond to different formulations for calculation of the wind speed climatology. Dashed lines correspond to results from repeated application of a single year of synoptic forcing. Results for the full integration domain are shown in the left panel, while results for the North Sea are displayed in the right panel. See the text for details.

initialized by the alternative formulation of the wind speed climatology, is depicted by the full thin line in Figure 6. The original results are given by the full thick line, and the horizontal line is the mean value for the final five years of the synoptically forced simulation. We find that the change in the computation of the wind speed climatology gives a very modest change in the model results. Further, the alternative wind speed climatology causes the initialization to be even further from the synoptically forced circulation.

Second, the results naturally raise the question of whether the climatology is suitable at all for initialization of ocean models at high latitudes, where the atmospheric variability is known to be high. In order to examine this topic, simulations were performed by repeated application of the synoptic forcing from a specific year. According to the North Atlantic Oscillation winter index, the extreme years in the present ten year period were 1995 and 1996. The results that were obtained for such an initialization are depicted by the thick and thin dashed lines in Figure 6, based on synoptic forcing from 1995 and 1996, respectively. When compared to the original initialization, we find that this alternative gives results that are significantly closer to the final five years of the synoptically forced ten year simulation.

5 Properties of ensemble variability

These simulations differed only in their initial states, which were taken from eight consecutive years in the climatologically forced simulation, as indicated in Figure 2. Since the ensemble members differ only in initial state, any differences between them can be attributed to nondeterministic differences in both the initial conditions and the evolution of the simulations. A technique to separate variability of a prognostic variable into two components was suggested by *Metzger et al.* [1994], and also used by *Melsom et al.* [2003]. The technique has been refined here. Consider results for a prognostic variable η at a point in space, and define a partitioning of η by

$$\eta_s(n) = \tilde{\eta}_s(d_n) + \hat{\eta}(n) + \eta'_s(n) \tag{4}$$

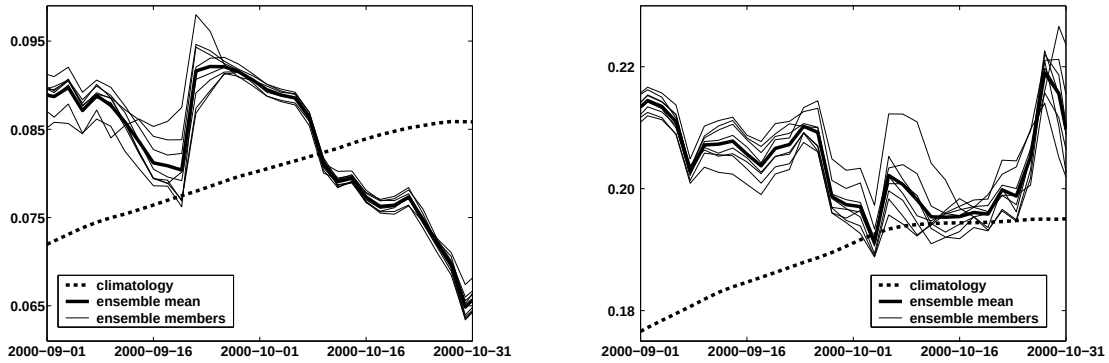

Figure 7: Baroclinic sea surface height (in m) during September and October 2000. Results shown in the left panel were extracted at 5° 26'E, 57° 13'N, southwest of Norway. To the right, results are displayed for 3° 50'E, 61° 42'N, near the west coast of Norway. The positions are indicated by white markers in Figure 3. Thin lines correspond to the eight members, and the thick solid and dashed lines correspond to the ensemble mean values and the daily climatologies, respectively.

where *s* is a realization in the set of ensemble simulations, which will hereafter be referred to as an ensemble member. Here, *n* is the time step, and d_n is the decimal day of time step *n*, as defined in Section 3.3. $\tilde{\eta}_s(d_n)$ is the daily climatology for member *s* on day d_n, based on model results from November 1996 – October 2001. A 30 day box filter was applied when the daily climatologies were computed. Further,

$$\hat{\eta}(n) = \frac{1}{S}\sum_{s=1}^{S}[\eta_s(n) - \tilde{\eta}_s(d_n)] \tag{5}$$

is the mean offset from the the daily climatologies. Then, from (4) we see that η' is the departure of each member from the instantaneous ensemble mean as a function of space and time so that

$$\overline{\eta'_s(n)}^s = \sum_{s=1}^{S}\eta'_s(n) = 0 \tag{6}$$

where the overbar corresponds to an average over the ensemble members.

Figure 7 displays the results for the baroclinic sea surface height at two locations in the eastern North Sea. The local daily climatology is given by the dashed lines, the eight ensemble members are depicted by thin solid lines, and the ensemble mean is shown as the thick solid line. Then, the offset $\hat{\eta}$ of the ensemble mean from the daily climatology is the distance from the dashed line to the thick solid line. The offset η'_s of ensemble member *no. s* from the ensemble mean is the distance from the thick solid line to the thin line that displays the results from this ensemble member.

Using (4) and (6), the mean square offset from the daily climatology ($\tilde{\eta}_s$) may be expressed as

$$\phi^2 = \frac{1}{S}\sum_{s=1}^{S}[\eta_s - \tilde{\eta}_s]^2 = \hat{\eta}^2 + \overline{\eta'^2_s}^s \tag{7}$$

Here, the final term on the right hand side is the instant local variance of the ensemble members. The first term on the right hand side is the local square offset of the ensemble mean from the daily climatology.

Keeping in mind that $\hat{\eta}$ is independent of the variability from one member to another, the temporal mean of $\hat{\eta}^2/\phi^2$ is an estimate of the fraction of deterministic variability in response to atmospheric forcing. The nondeterministic variability fraction which is due to flow instabilities, is then given by

the mean of $\overline{\eta_s'^2}^s/\phi^2$. This fraction enables us to quantify the contribution from nondeterministic variability as a fraction between 0 and 1. Note that the accuracy of these estimates depends on the ensemble's size.

Re-examining the results that were depicted in Figure 7, we may illustrate the terms on the right hand side of Equation 7. In Figure 8, the ensemble variance and the square offset from the daily climatology are depicted as functions of time by the thick and thin lines, respectively.

6 Ensemble size

As previously stated, the suite of ensembles is made up of a total of eight members. In this section, we will investigate how the ensemble size affects the interpretation of the results, by comparing the full ensemble set to subsamples. This investigation will be based on the overall mean value for the fraction of nondeterministic variability of the baroclinic sea surface height,

$$\overline{\mu_\zeta}^n = \frac{1}{N}\sum_{n=1}^{N}\mu_{\zeta_n} = \frac{1}{N}\sum_{n=1}^{N}\left[\frac{1}{T}\sum_{t=1}^{T}\frac{(\overline{\eta_{\zeta_s}'^2}^s)_t}{(\phi_\zeta^2)_t}\right]_n \tag{8}$$

Here, μ_{ζ_n} is the fraction of nondeterministic variability at wet grid node *no.* n, and t corresponds to the time step. T and N are the total number of time steps considered and the total number of wet grid nodes, respectively. The results for μ_ζ are displayed in Figure 9, the maximum value is 0.36. However, the largest values are found in the region to the south and southwest of the outflow port. Hence, these values may be associated with nonlinear processes that are related to the configuration of the experiment. The maximum value in the North Sea and the Skagerrak is 0.16. Further, we will also consider the spatial variance of μ_ζ,

$$\sigma_{\mu_\zeta}^2 = \frac{1}{N}\sum_{n=1}^{N}(\mu_{\zeta_n} - \overline{\mu_\zeta}^n)^2 \tag{9}$$

The ensemble members were initiated from eight consecutive years from the preceding simulation with climatological forcing, as indicated by the open circles in Figure 2. If the variability of the results produced with climatological forcing has a memory on a time scale of a year or more, we

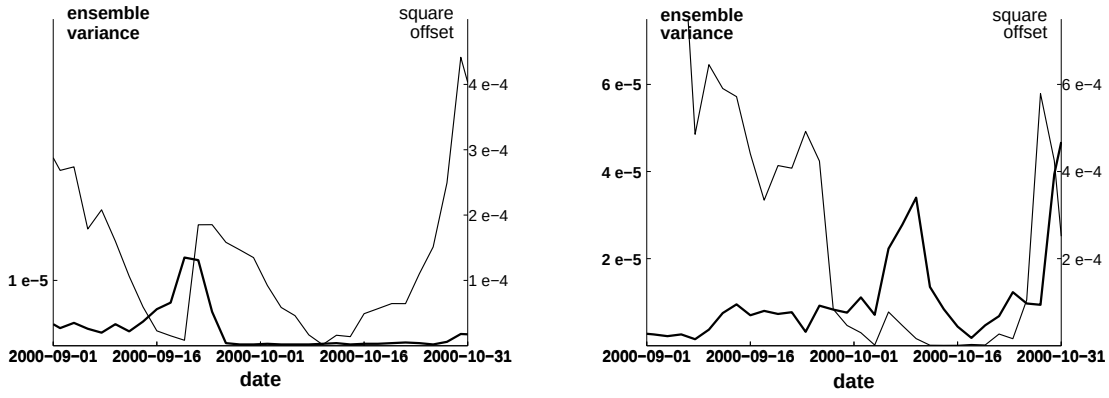

Figure 8: The ensemble variance (thick line) and the square offset from the daily climatology (thin line), based on the same results as Figure 7. Values along the vertical axes are in m^2. Note that the resolution along the vertical axes differ by a factor of 10.

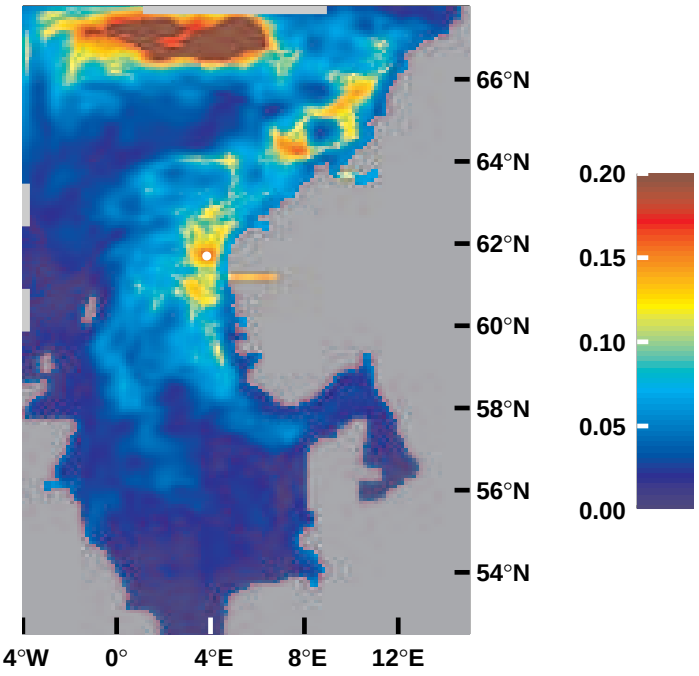

Figure 9: The fraction of nondeterministic variability (μ_ζ) for the baroclinic sea surface height. The color coding is shown by the color bar in the right panel. The white marker is at the same position as the northernmost marker in Figure 3.

expect that the differences between two consecutive ensemble members (*i.e.*, members initialized from consecutive years from the climatologically forced simulation) will be smaller than the differences of other ensemble member combinations. Hence, we compute results for $\overline{\mu_\zeta}^n$ and $\sigma^2_{\mu_\zeta}$, for various sets of two member mini-ensembles. The results are displayed in Figure 10, with full circles corresponding to pairs of consecutive members, and open circles and open squares corresponding to pairs that were initiated 3 and 5 years apart, respectively. The results displayed in the left panel of Figure 10 show that on average, the values are slightly smaller for consecutive ensemble members. This indicates that

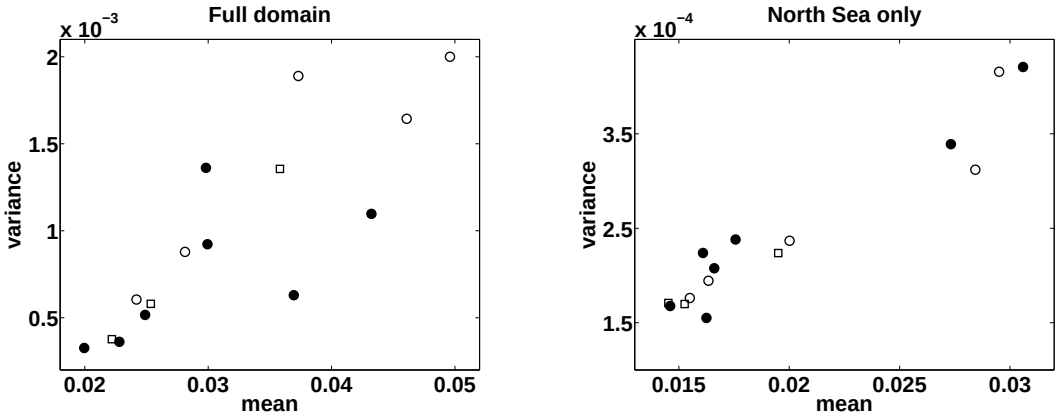

Figure 10: Variability based on various combinations of pairs of ensemble members: Consecutive members (full circles), and members that were initiated three years and five years apart (open circles and open squares, respectively). The x-axis corresponds to the overall mean fraction of nondeterministic variability, and values along the y-axis show the spatial variance of this fraction. Results for the full integration domain are shown in the left panel, while results for the North Sea are displayed in the right panel.

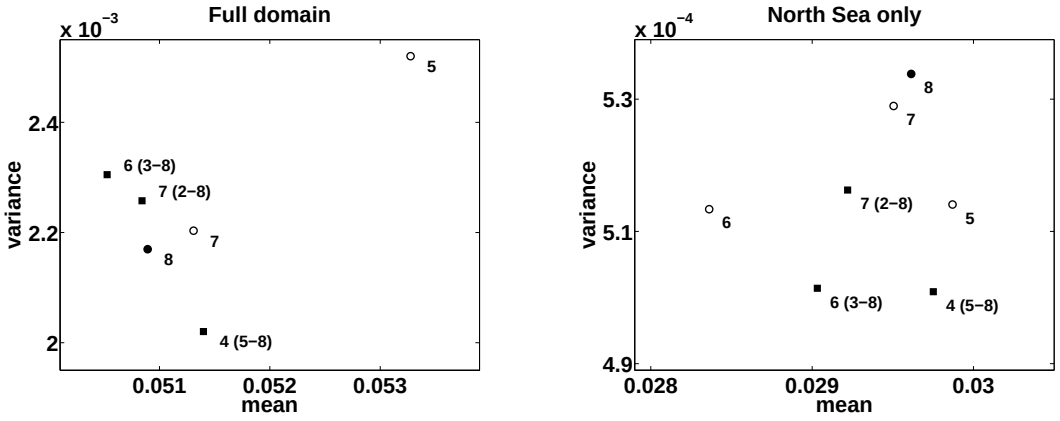

Figure 11: Results for various ensemble sizes, and for various combinations of ensemble members. Results obtained for ensembles with members initiated from consecutive and non-consecutive years from the climatological spin-up is represented by full circles and open squares, respectively. The symbols' labels denote the ensemble size. The range of the members' numbers is given in the parenthesis for the consecutive ensemble sets. The remaining sets were composed as follows: 7 members: 1-3,5-8; 6 members: 1,2,4,5,7,8; 5 members: 1,3,5,6,8; 4 members: 2,4,6,8. The x- and y-axes correspond to the same properties as in Figure 10, and the left and right panels are again for the full domain and for the North Sea, respectively.

the memory may exceed one year when the full model domain is considered, but the differences are small. The results for the North Sea in the right panel is not suggestive of a memory that exceeds one year in this sub-domain. Different lengths of memory may be due to slower spin-down by bottom friction in the deep ocean.

Further, the results are examined by composing ensembles of various sizes from the eight members that are available: In addition to the full ensemble set, sets of 4, 5, 6, and 7 members are examined. For each ensemble size, the members were organized according to two different strategies, using either consecutive members, or using a spread of ensemble member numbers. The results are displayed in Figure 11, and the composition of the various sets are specified in the figure caption.

From the present ensemble set, we generally find that, with respect to the properties $\overline{\mu_\zeta}^n$ and $\sigma^2_{\mu_\zeta}$ of the fraction of nondeterministic variability, convergence is not more rapid when a spread of ensemble member numbers are considered than for consecutive members. We also find that both of the properties $\overline{\mu_\zeta}^n$ and $\sigma^2_{\mu_\zeta}$ tend to increase as the size of the ensemble increases, although not uniformly. Moreover, the present results suggest that their values are converging rapidly for ensembles that are composed of more than six members. A more accurate description of how the ensemble convergence for various ensemble sizes relates to natural variability requires precise observations and use of methods such as rank histograms (*Hamill*, 2001), although that method may not be suited for this type of ensemble simulations (*Melsom*, 2004).

7 Relations between wind forcing and ensemble variability

In this section we will examine the relations between the momentum flux from the atmosphere to the ocean, the variability of the kinetic energy associated with the baroclinic modes, and the baroclinic sea surface height variability. Our goal is to determine whether or not a relation exists between wind forcing that piles up water in the Skagerrak, and oceanic variability in the North Sea off the west coast of Norway. This investigation will be performed by computation of correlations between time series

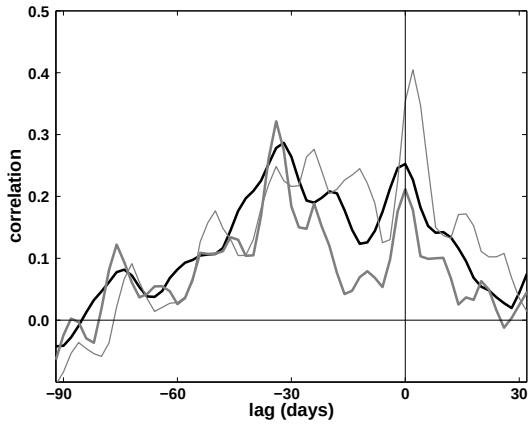

Figure 12: Lagged correlations between the air-sea momentum flux in the Skagerrak and oceanic variability in the eastern North Sea (4° 19'E, 60° 40'N). The black line displays the correlations between southerly winds in the Skagerrak and $\overline{\eta_s'^2}^s{}_\zeta$. The corresponding results for $\overline{\eta_s'^2}^s{}_{E^{eddy}}$ is depicted by the thick gray line, while the thin gray line shows the correlations between wind and $\hat{\eta}^2{}_{E^{eddy}}$. Lags along the *x*-axis are in days, with positive values corresponding to momentum flux lagging the baroclinic sea surface height. Only episodes with winds from the south were considered.

of momentum flux from the atmosphere in the Skagerrak, and the variability of the kinetic energy associated with the baroclinic modes, and the baroclinic sea surface height variability, in a position in the eastern North Sea (4° 19'E, 60° 40'N). The front between the Norwegian Coastal Current and saltier water to the west is frequently close to this position. As mentioned in section 1, we know that mesoscale features like meanders and eddies are abundant in this region. Such nonlinear phenomena are likely to lead to a relatively high fraction of nondeterministic variability.

In order to single out events where water is piled up in the Skagerrak, only periods with winds from the south are considered. Furthermore, only the north-south component of the atmospheric momentum flux is considered when the correlations are computed. The results are displayed in Figure 12, where the black line displays the lagged correlation between winds from the south in the Skagerrak, and the ensemble variance of the baroclinic sea surface height ($\overline{\eta_s'^2}^s{}_\zeta$) for the selected position in the eastern North Sea. The corresponding results for $\overline{\eta_s'^2}^s{}_{E^{eddy}}$ are given by the thick gray line. The thin gray line displays the lagged correlations between the atmospheric momentum flux and the squared offset of the eddy kinetic energy ensemble mean from its daily climatology ($\hat{\eta}^2{}_{E^{eddy}}$). Lags in Figure 12 are positive when oceanic variability leads the winds. The quoted quantities of ensemble variability were defined in Equations (4)-(7).

From Figure 12, we observe that the lagged correlations exhibit a two-peak structure. One peak is found at approximately no lag, while another peak is found with the Skagerrak winds leading the oceanic variability by about a month. The former peak is almost certainly the local response of the ocean's state to the same atmospheric pressure system that gave rise to the southerly winds in the Skagerrak. The latter peak is probably due to a propagating oceanic signal. In section 8, these results will be related to earlier investigations of relevance here.

In the present context it is important to realize that the highest correlation values are moderate, about 0.3. Hence, during and after wind events that pile up water in the Skagerrak, only about 10% of the presently considered properties of oceanic variability can be explained by the variability of the southerly wind component. So, we did not discover a dominating impact on the ensemble variability off the coast of southern Norway.

The fractions of nondeterministic variability at the selected position were 0.10 and 0.13 for the baroclinic sea surface height and for the eddy kinetic energy, respectively. The modest values for these fractions may be related to the horizontal resolution, 9 km, which is too coarse to resolve most mesoscale features in this region.

8 Discussion and concluding remarks

As discussed in section 4, the choice of strategy for model initialization is not trivial. Although it was not our original intention, an effort was made in order to explore various approaches for model initialization, and to examine the subsequent adjustment when applying synoptical forcing fields. All synoptically forced simulations were initialized from fields produced by application of monthly climatologies for atmospheric forcing. We found that this approach leads to an underestimation of the spatial variability. Better estimates are produced by repeated application of a single year of atmospheric forcing. Hence, with the benefit of hindsight we should have opted for the latter approach. The results suggest that the initial spread in spatial variability due to arbitrary choosing one particular year for model initialization (Figure 6, left panel), is comparable to the year-to-year variability of the same quantity (Figure 5, left panel). Hence, when the latter approach is selected, we could safely have included at least the final eight years of the ten year simulation period in our analysis. Unfortunately, climatological forcing was applied to spin up our simulations, and we are left with only five years with model results that are suitable in the present analysis.

An important part of this study is the quantification of nondeterministic variability in the North Sea and the Skagerrak in general, and in the Norwegian Coastal Current in particular. For this purpose, we have examined simulation results for two quantities, the baroclinic sea surface height anomalies (a measure of the dynamic height), and the eddy kinetic energy associated with the baroclinic modes. These quantities were selected since their variability is well-resolved in time, and since they are vertically integrated (two dimensional in space) measures of variability in three spatial dimensions. Generally, the analysis of one of these quantities give results that are similar to the corresponding analysis of the other. One example is that the correlation of the ensemble variance $\overline{\eta_s'^2}^s$ time series of the two quantities at the position 4° 19'E, 60° 40'N in the eastern North Sea is 0.86. This is not surprising, in an isopycnic framework the baroclinic sea surface height is determined by the distribution of the layers, while the baroclinic velocity components are proportional to the horizontal gradients of the same distribution.

The model initialization problem is due to the circumstance that the ocean circulation variability at the present latitudes is dominated by relatively high frequencies that arise due to the character of the synoptic atmospheric forcing. This is not only seen in the fast barotropic mode but also in the much slower baroclinic modes, *e.g.* as revealed by the peak at no lag in Figure 12. Hence, there is a possibility that the variability of both the baroclinic sea surface height anomalies and the eddy kinetic energy of the baroclinic modes are significantly affected, if not dominated, by the rapid variations in the atmospheric forcing fields. The mesoscale variability may affect these quantities less than we originally assumed. From the definition in Equation 2, we note that the eddy kinetic energy is only an expression of the temporal variability of the kinetic energy locally. More suitable information about the intensity of the mesoscale may be derived by analyzing the relative vorticity. Results of such an analysis will be reported in an upcoming publication (*Melsom*, 2004). Another relevant issue in this context, is the horizontal resolution, which is on the coarse side when it comes to resolving mesoscale structures like eddies. *Melsom* (2004) will present results for the same domain, from simulations with four times as many grid points in *x*,*y*-space compared to the present case.

In their investigation of eddies off the coast of southern Norway, *Furnes et al.* (2001) find that the intensity of eddies are largest after a change in the wind condition in the Skagerrak. They suggest that the formation of intense eddies are related to the propagation of a front along the Norwegian coast. West of Lista at the southern tip of Norway, the propagation speed of this front is about 25 km/day. Interestingly, the lagged correlations with Skagerrak winds in section 7 reveal that the oceanic signal at a specific position in the eastern North Sea lags the winds by about one month. This particular position

is at a distance of about 500 km from the Skagerrak. Since the outbreak of the front is probably delayed by some days relative to the wind maximum, the present results indicate a propagation speed of about 20 km/day.

The investigation by *Furnes et al.* (2001) was prompted by an incident at the oil rig *West Venture* in the afternoon hours of 18 November 2000. The oil rig, which was then position in the region of the *Troll* field, drifted off its position due to a combination of strong winds and strong currents, and the drilling operation had to be stopped. *West Venture*'s position (3° 35'E, 60° 51'N) is displayed by the white marker in the figure on the cover page of this report. We note that this is near a steep gradient in the baroclinic sea surface height anomalies in the model results. Due to the quasi-geostrophic conditions in the ocean, such gradients will be accompanied by strong baroclinic currents.

From the results depicted in Figure 3 we found that the coastal wave guide is a region where the baroclinic sea surface height variance is high. However, the square offset of the ensemble mean from the climatology is also high in this region, so higher fractions of nondeterministic variability is found to the west of the coastal wave guide, as revealed by Figure 9. Another example of this, is that while the fraction of nondeteministic variability has a local maximum at the position of the white marker in Figure 9, the variance has a local minimum at the same position (see Figure 3). The fractions of nondeterministic variability are highest in the frontal regions associated with the model's representation of the Norwegian Coastal Current and the Norwegian Atlantic current. There, small differences in the initial fields may give rise to differences in the model results that account for about 5% - 15% of the total variance. Further to the west, both the ensemble variance and the fraction of nondeterministic variability are low. Note that these results are for a horizontal resolution of approximately 9 km, the dependence of the results on model resolution will be discussed by *Melsom* (2004).

Acknowledgment.

I would like to thank E. Joseph Metzger (Navy Research Laboratory, Stennis, MS) for introducing me to the concept and interpretation of ensembles of model experiments. NCEP Reanalysis data were provided by the NOAA-CIRES Climate Diagnostics Center, Boulder, Colorado, USA, from their Web site at http://www.cdc.noaa.gov/ This study has been financed by the Norwegian Research Council under contract *no.* 146476/120. Computer time on a SGI Origin 3000 at the Norwegian high performance computing facility was granted by the Norwegian Research Council. However, most of the computations were performed at the Norwegian Meteorological Institute's IBM Linux cluster. Thanks to Trond P. Bø at the institute for help to configure HYCOM at the cluster. Also thanks to Alan J. Wallcraft (Navy Research Laboratory, Stennis, MS) for providing a recent version of HYCOM at an early stage, and for assistance toward trouble shooting. Øyvind Sætra at the Norwegian Meteorological Institute provided a number of very helpful suggestions, and his contribution is greatly appreciated.

References

Aure, J., and R. Sætre, 1981: Wind effects on the Skagerrak outflow. In *The Norwegian Coastal Current. Proceedings Norwegian Coastal Current symposium*, Eds. R. Sætre and M. Mork, Univ. Bergen, Bergen, Norway, 263-293.

Bleck, R., 2002: An oceanic general circulation model framed in hybrid isopycnic-cartesian coordinates. *Ocean Modelling, 4*, 55-88.

Bleck, R., C. Rooth, D. Hu, and L. T. Smith, 1992: Salinity thermocline transients in a wind- and thermohaline-forced isopycnic coordinate model of the Atlantic Ocean. *J. Phys. Oceanogr., 22*, 1486-1505.

Browning, G. L., and H.-O. Kreiss, 1982: Initialization of the shallow water equations with open boundaries by the bounded derivate method. *Tellus, 34*, 334-351.

Chassignet, E. P., L. T. Smith, G. R. Halliwell, and R. Bleck, 2003: North Atlantic simulations with the HYbrid Coordinate Ocean Model (HYCOM): Impact of the vertical coordinate choice, reference pressure, and thermobaricity. *J. Phys. Oceanogr., 33*, 2504-2526.

Dooley, H. D., and G. K. Furnes, 1981: Influence of the wind field on the transport of the Northern North Sea. In *The Norwegian Coastal Current. Proceedings Norwegian Coastal Current symposium*, Eds. R. Sætre and M. Mork, Univ. Bergen, Bergen, Norway, 57-71.

Engedahl, H., 1995: Implementation of the Princeton Ocean Model (POM/ECOM3D) at the Norwegian Meteorological Institute (DNMI). *Research Rep. No. 5*, Norwegian Meteorological Institute, Oslo, Norway, 40 pp.

Engedahl, H., B. Ådlandsvik, and E. A. Martinsen, 1998: Production of monthly mean climatological archives for the Nordic Seas. *J. Marine Systems, 14*, 1-26.

Furnes, G. K., H. Engedahl, D. Hareide, and J. Aure, 2001: Strømvirvler langs kysten av sør-Norge: Et tilbakeblikk på hendelsen ved Trollfeltet 18. november 2000 (*Ocean eddies along the coast of southern Norway: Looking back on the 18 November 2000 event at the Troll field.*). *Norsk Hydro Rep. ID NH-00039406*, Norsk Hydro Sandvika, Norway, 22 pp.

Hallberg, R., 2000: Time integration of diapycnal diffusion and Richardson number mixing in isopycnal coordinate ocean models. *Mon. Weather Rev., 128*, 1402-1419.

Hamill, T. M., 2001: Interpretation of rank histograms for verifying ensemble forecasts. *Mon. Weather Rev., 129*, 550-560.

Halliwell, G. R., 2003: Evaluation of vertical coordinate and vertical mixing algorithms in the HYbrid Coordinate Ocean Model (HYCOM). *Ocean Modelling*, in press.

Jerlov, N. G., 1976: Marine Optics. Elsevier Oceanography Series, Elsevier Sci. Publ. Co., New York. 231 pp.

Kraus, E. B., and J. S. Turner, 1967: A one-dimensional model of the seasonal thermocline: II. The general theory and its consequences. *Tellus, 19*, 98-106.

Large, W. G., J. C. McWilliams, and S. C. Doney, 1994: Oceanic vertical mixing: A review and a model with a nonlocal boundary layer parameterization. *Rev. Geophys., 32*, 363-403.

Martinsen, E. A., B. Hackett, L. P. Røed and A. Melsom, 1997: Operational marine models at the Norwegian Meteorological Institute. In *Operational Oceanography. The Challenge for European Co-operation*, Eds. J. H. Stel, H. W. A. Behrens, J. C. Borst, L. J. Droppert and J. v.d. Meulen, *Elsevier Oceanogr. Ser., 62*, 436-443.

Martinsen, E. A., A. Melsom, V. Sveen, E. Grong, M. Reistad, N. Halvorsen, Ø. Johansen and K. Skognes, 1994: The operational oil drift system at DNMI. *Technical Report No. 125*, Norwegian Meteorological Institute, Oslo, Norway, 52 pp.

McDougall, T. J., and W. K. Dewar, 1998: Vertical mixing, cabelling and thermobaricity in layered models. *J. Phys. Oceanogr., 28*, 1458-1480.

Melsom, A., 2004: Ensemble simulations and the ocean's mesoscale. Submitted to *Ocean Dyn.*

Melsom, A., E. J. Metzger, and H. E.Hurlburt, 2003: Impact of remote oceanic forcing on Gulf of Alaska sea levels and mesoscale circulation. *J. Geophys. Res., 108*(C11), 3346 doi: 10.1029/2002JC001742.

Metzger, E. J., and H. E.Hurlburt, 2001: The nondeterministic nature of Kuroshio penetration and eddy shedding in the South China Sea. *J. Phys. Oceanogr., 31*, 1712-1732.

Metzger, E. J., H. E. Hurlburt, G. A. Jacobs, and J. C. Kindle, 1994: Hindcasting wind-driven anomalies using reduced-gravity global ocean models with 1/2 and 1/4 resolution. *NRL Tech. Rep. 9444*, 21 pp., Nav. Res. Lab., Stennis Space Center, Miss.

Røed, L. P., and I. Fossum, 2004: Mean and eddy motion in the Skagerrak/ northern North Sea: insight from a numerical model. *Ocean Dyn.*, 54, 197-220.

Shi, X. B., L. P. Røed, and B. Hackett, 2001: Variability of the Denmark Strait overflow: A numerical study. *J. Geophys. Res.*, *106*, 22,277-22,294.

Sætra, Ø., and C. Wettre, 2000: Simulations of the Braer Drift. *Research report No. 72*, Norwegian Meteorological Institute, Oslo, Norway, 27 pp.

Sætre, R., 1983: Ocean currents in the upper layers off Norway. (In Norwegian). Rep. no. FO 8306, Inst. of Mar. Res., Bergen, Norway.

Wettre, C., Ø. Johansen, and K. Skognes, 2001: Development of a 3-dimensional oil drift model at DNMI. *Research Rep. No. 133*, Norwegian Meteorological Institute, Oslo, Norway, 50 pp.